Supporting Information

One-step synthesized iron foam based $NiFe_2O_4$ applied for self-powered water splitting hydrogen production

Juan Jian,[a] Yufeng Zhang,[a] Zhuo Wang,[a] Xinxin Zheng,[a] Ping Nie[a], Wanting Yang[a], Tianhui Zhang[a] and Limin Chang[a,*]

[a] Key Laboratory of Preparation and Applications of Environmental Friendly Material of the Ministry of Education, College of Chemistry, Jilin Normal University, Changchun 130103, P. R. China

[b] State Key Laboratory of Inorganic Synthesis and Preparative Chemistry, College of Chemistry, Jilin University, Qianjin Street 2699, Changchun 130012, P. R. China

* Corresponding author's E-mail: changlimin2139@163.com

1. Material and Experimental Instruments

1.1 Materials used in the experiment

Pt/C (20 wt%) was obtained from Macklin Ltd. (Shanghai, China), RuO_2 was synthesized from ruthenium chloride hydrate ($RuCl_3 \cdot xH_2O$) purchased from Aladdin Ltd. (Shanghai, China).[1] Nickel foam (NF) and Iron foam (IF) were provided by the Li Yuan Technology Co. Ltd. (Shanxi, China). KOH, CH_4N_2O, HCl and other chemicals are supplied by the Beijing Chemical Reagents Company. Apart from the NF and IF, all the chemicals are analytical pure and do not needed further purification.

1.2 Experimental Section

Basic Phase Characterizations

X-ray diffraction (XRD) experiment was tested on a Rigaku D-Max 2550 diffractometer with Cu-Kα radiation (λ = 1.5418 Å). Scanning electron microscope (SEM) and energy dispersive X-ray spectroscopy (EDX) images were obtained on a JEOL-6700 scanning electron microscope. Transmission electron microscope (TEM), high resolution TEM (HRTEM) images were obtained with microscopy of Philips-FEI Tecnai G2S-Twin, equipped with a field emission gun operating at 200 kV. X-ray photoelectron spectra (XPS) analysis was performed on a VG Scienta R3000 spectrometer with Al Kα (1486.6 eV) as the X-ray source.

Electrochemical Measurements

The electrochemical measurements were conducted using the three-electrode system with the electrochemical workstation (CHI 760e). The as-prepared electrodes were directly used as the working electrodes; meanwhile, graphite rod and Hg/HgO electrode were served as counter and reference electrodes, respectively. 1.0 M KOH solution was used as electrolyte for HER, OER and OWS devices, while 0.1 M KOH were applied for the ORR process. Potentials were normalized versus the standard hydrogen electrode (RHE) according to formula below:

$$E_{(RHE)} = E_{(Hg/HgO)} + 0.098\ V + 0.0591\ pH \quad (1)$$

Here, "$E_{(Hg/HgO)}$" is the potential we directly measured during the experiment.

Polarization curves were performed via sweeping potentials at a scan rate of 2.0 mV s^{-1}.

Tafel slope:

The data of Tafel slope can be plotted by the gained linear sweep voltammetry (LSV) curves, which is obtained from the equation below:

$$\eta = a + b \log j \quad (2)$$

Where, "η" refers to the overpotential; "j" is the current density; "a" relates to the j_0 (exchange current density) and can be reflected by the intercept; "b" is the Tafel slope we need to achieve.

Electrochemical active surface area (ECSA)

The ECSA is calculated by the formula below:

$$ECSA = A * C_{dl} / C_s \quad (3)$$

Herein, "A" refers to the area of the working electrode, and we set the electrode area to 0.25 cm^2 throughout the electrocatalytic water splitting testing; "C_s" relates to the electrolyte and C_s = 0.04 mF cm^{-2}, "C_{dl}" is the abbreviation of double layer capacitance and calculated from a series of CV curves that tested within the non-Faraday potential range (0.9254-1.0254 V vs. RHE), scan rate changed from 10 to 100 mV s^{-1}, increased with 10 mV s^{-1} each time.

Assembly and Testing of the Zn-Air Battery

As for the liquid Zn-air battery, to avoid electrolyte leakage, we physically compounded the IF-based catalyst with the waterproof/breathable carbon film, and then assembled the complex as the air-cathode of the liquid Zn-air battery.[2] In addition, the working area of the Zn-air battery is 0.19625 cm^2, for that the semidiameter of the air-cathode side is 0.25 cm.

The charge and discharge curves were measured by the CHI 760e, the power density was calculated from the data of the discharge curve. Charging-discharging cycling curves at current density of 10 mA cm^{-2} in this work were measured by the Land battery test system.

2. Theoretical Section

Computation Details

The density functional theory (DFT) calculations were performed using the Vienna Ab initio Simulation Package (VASP)[3,4], with the generalized gradient approximation (GGA) Perdew–Burke–Ernzerhof (PBE) functional[5] to describe electron exchange and correlation. The projector-augmented plane wave (PAW)[6,7] potentials were used to describe the core-valence electron interaction and take valence electrons into account using a plane wave basis set with a kinetic energy cutoff of 500 eV. Partial occupancies of the Kohn−Sham orbitals were allowed using the Gaussian smearing method and a width of 0.05 eV. Electronic energy was considered self-consistent when the energy change was smaller than 10^{-5} eV. A geometry optimization was considered convergent when the force change was smaller than 0.02 eV/Å. A k-points

sampling of 1 × 2 × 1 with Monkhorst-Pack [8] scheme was used in all calculations and all calculations were considered the spin polarization effect.

The $NiFe_2O_4$ (311) slab surface was generated as the adsorption model. After the slab model was constructed, the intermediates of H, OH, O, and OOH groups were absorbed on the Fe or Ni sites, respectively, to evaluate its HER and OER properties.

The adsorption energy Δ*E* for *A* = OH, O, and OOH groups on the surfaces of substrates was defined as:

$$\Delta E = E_{*A} - (E_{*} + E_{A}) \quad (4)$$

where *A and * denote the adsorption of A groups on substrates and the bare substrates, while E_A denotes the energy of A groups.

The free energy change ΔG of the reaction was calculated as the difference between the free energies of the initial and final states, as shown below:

$$\Delta G = \Delta E + \Delta ZPE - T\Delta S \quad (5)$$

where ΔE is the energy change between the reactant and product obtained

from DFT calculations, ΔZPE is the change in the zero-point energy; T and ΔS denote the temperature and the change of entropy, respectively. Herein, T = 300 K was considered.

The electrochemical model of the oxygen evolution reaction / oxygen reduction reaction (OER / ORR) in alkaline media could be divided into four one-electron reactions:

$$^{*} + OH^{-} \leftrightarrow {}^{*}OH + e^{-} \quad (6)$$

$$^{*}OH + OH^{-} \leftrightarrow {}^{*}O + H_2O(l) + e^{-} \quad (7)$$

$$^{*}O + OH^{-} \leftrightarrow {}^{*}OOH + e^{-} \quad (8)$$

$$^{*}OOH + OH^{-} \leftrightarrow {}^{*} + O_2(g) + H_2O(l) + e^{-} \quad (9)$$

where the * denotes the active site. The adsorption energies of intermediates (OH, O, and OOH groups) on substrates were calculated by the following equations:

$$\Delta E_{*O} = E_{(sub/O)} - E_{(sub)} - [E_{(H2O)} - E_{(H_2)}] \quad (10)$$

$$\Delta E_{*OH} = E_{(sub/OH)} - E_{(sub)} - [E_{(H2O)} - E_{(H2)}/2] \quad (11)$$

$$\Delta E_{*OOH} = E_{(sub/OOH)} - E_{(sub)} - [2 \times E_{(H2O)} - 3 \times E_{(H2)}/2] \quad (12)$$

Where $E_{(sub/H2O)}$, $E_{(sub/OH)}$, $E_{(sub/O)}$ and $E_{(sub/OOH)}$ denoted the total energies of H_2O, OH, O, and OOH groups on substrates. $E_{(sub)}$, $E_{(H2O)}$, and $E_{(H2)}$ were the energies of the bare substrate, water, and hydrogen gas, respectively.

The Gibbs free energy changes of Equations (6-9) could be estimated by:

$$\Delta G_1 = \Delta G_{*OH} \quad (13)$$

$\Delta G_2 = \Delta G_{*O} - \Delta G_{*OH}$ (14)

$\Delta G_3 = \Delta G_{*OOH} - \Delta G_{*O}$ (15)

$\Delta G_4 = 4.92eV - \Delta G_{*OOH}$ (16)

where the sum of $\Delta G_{1\text{-}4}$ was fixed to the negative of the experimental Gibbs free energy of the formation of two water molecules. The Gibbs free energy of ($H^+ + e^-$) in solution was estimated as half the energy of the H_2 molecule in the standard condition.

The overpotential of the OER was determined by the following Equations:

$\eta = U_{OER} - 1.23$ (17)

$U_{OER} = Max(\Delta G_1, \Delta G_2, \Delta G_3, \Delta G_4) /e$ (18)

3. Supplementary Figures and Tables

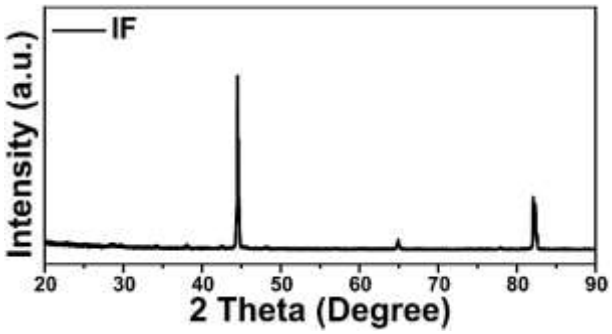

Fig. S1. The XRD data of bare IF.

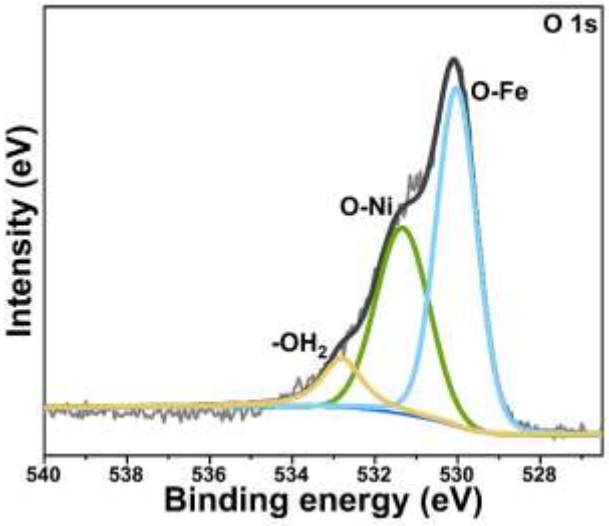

Fig. S2. The O 1S spectra of $NiFe_2O_4$.

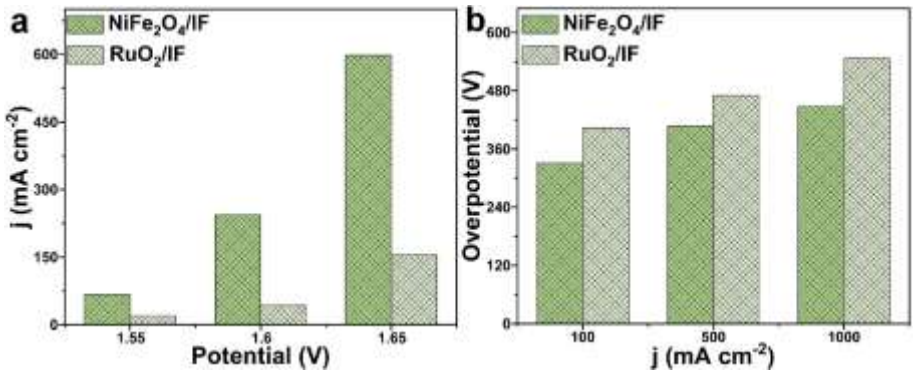

Fig. S3. The contrast bar graphs between potential and current density of $NiFe_2O_4$/IF and RuO_2/IF during the OER course.

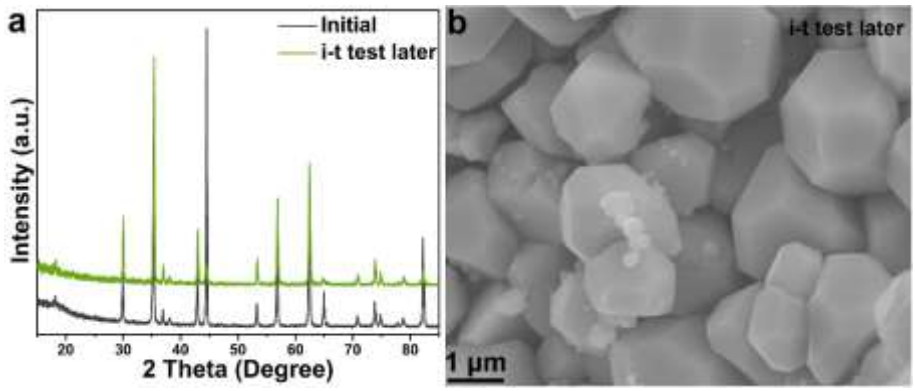

Fig. S4. The XRD data and SEM image of $NiFe_2O_4$/IF the i-t test later during the OER course.

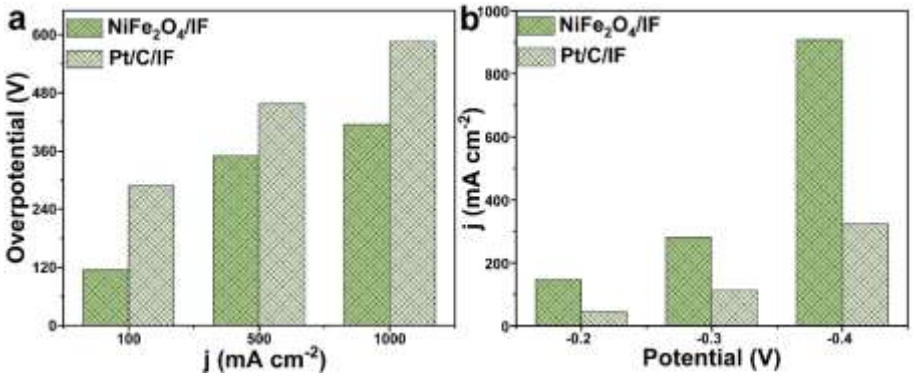

Fig. S5. The contrast bar graphs between potential and current density of $NiFe_2O_4$/IF and RuO_2/IF during the HER process.

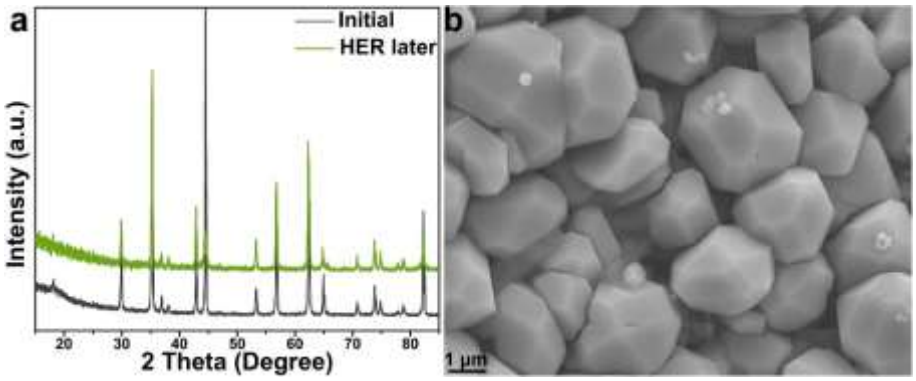

Fig. S6. The XRD and the SEM results of $NiFe_2O_4$/IF that the HER test later.

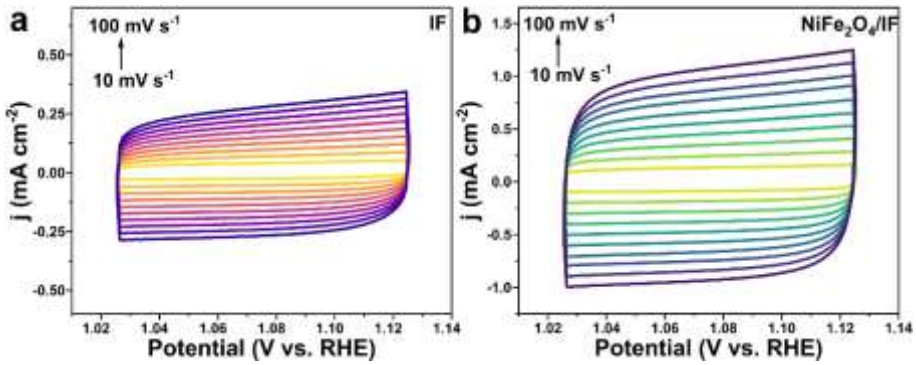

Fig. S7. The cyclic voltammetry (CV) curves of bare IF, $NiFe_2O_4$/IF when the scan rates changed from 10 to 100 mV s^{-1} and increased at a rate of 10 mV s^{-1} each time.

Table S1. C_{dl}, ECSA and related data of bare IF and $NiFe_2O_4$/IF.

Catalyst	C_{dl} (mF cm^{-2})	C_s (mF cm^{-2})	A (cm^2)	ECSA (cm^2)
IF	2.16	0.04	0.25	13.50
$NiFe_2O_4$/IF	9.91	0.04	0.25	61.94

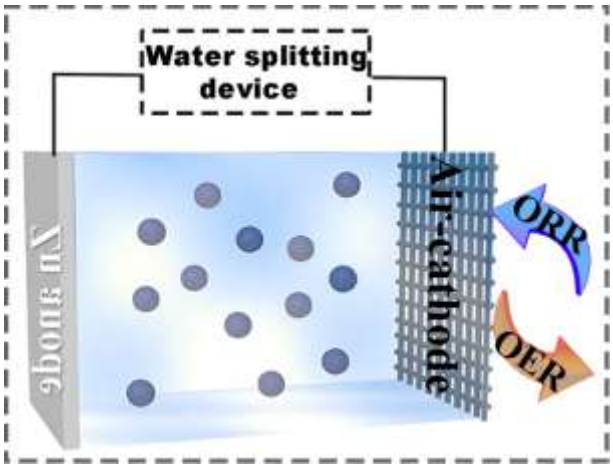

Fig. S8. The structural schematic diagram of liquid ZAB.

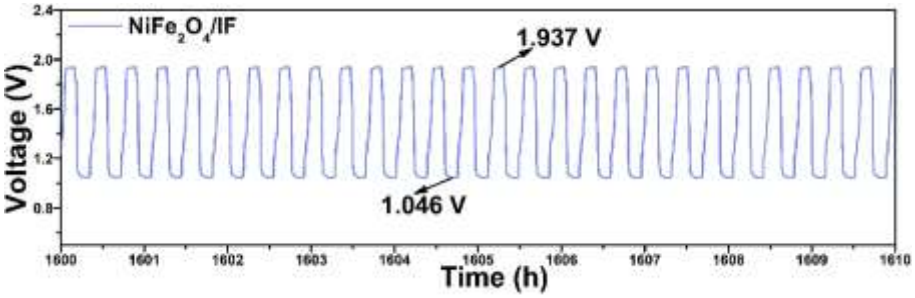

Fig. S9. The enlarged view that charging-discharging cycling curves between 1600 and 1610 h of Fig. 6c.

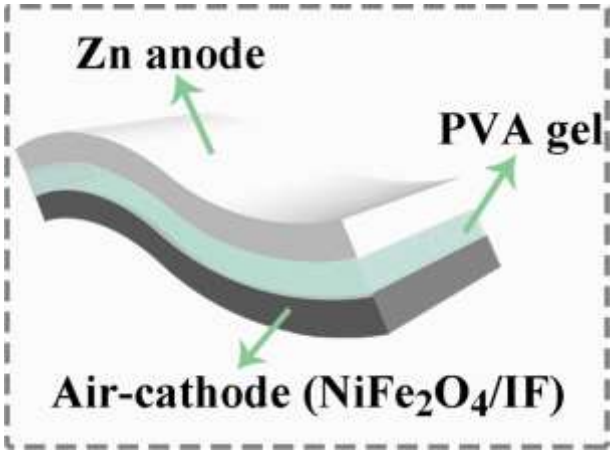

Fig. S10. The structural schematic diagram of flexible ZAB.

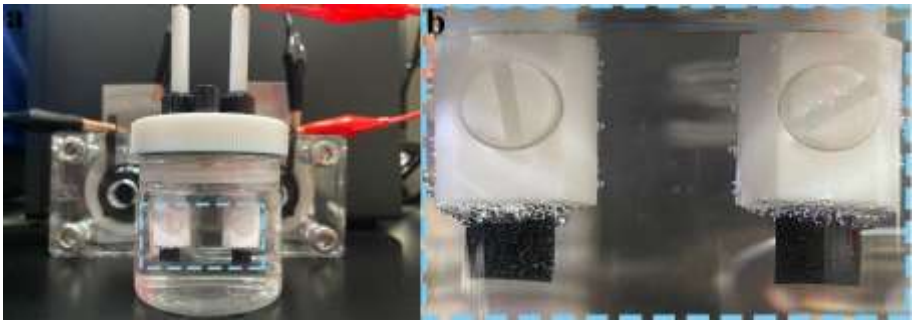

Fig. S11. The photographs of the self-powered water splitting device and corresponding enlarged image.

Table S2. A conclusion of the Zn-air battery activities for the recently reported self-powered trifunctional catalysts.

Trifunctional catalyst	Voltage @ 10 mA cm^{-2} (OWS)	Power density (mW cm^{-2})	Charging and discharging cycle time @ 10 mA cm^{-2} (h)	Voltage gap (V)	Reference
$NiFe_2O_4$/IF	**1.518**	**138.1**	**> 1600**	**0.817**	**This work**
Pt/C+RuO_2/IF	1.54	95.4	170	0.881	This work
NiCoP/NiO	1.71	84.5	113	0.84--0.86	[9]
Fe-NiCoP	1.60	--	900 cycles @ 5 mA cm^{-2}	--	[10]
Fe Doped MOF CoV@CoO nanoflakes	1.53	138	50	0.89	[11]
Co-MOF-800	--	144	85 @ 1 mA cm^{-2}	0.46--0.58	[12]
Co@NCL	1.70	170	200	0.88	[13]
Co/N-CNF-800	1.80	--	50	1.39	[14]
3%IrO_x/NCNT	1.52	59.3	120 @ 5 mA cm^{-2}	0.65	[15]
CoFe@NC/NCHNSs-700	1.66	184	50	~0.87	[16]
CoDNG900	--	205.6	667	0.82	[17]
Pt/d-CoP/NPC	1.53	182.8	200	~1.05	[18]
MoCoP-NPC	1.65	175.2	300	0.47--0.5	[19]
$FeZn_4Co$@CNFs	--	107.6	118	~0.87	[20]
Co-COP	--	83.6	--	--	[21]
SC-Cu_{SA}-NC	1.58	124.9	120	~0.9	[22]

Fe-N-C/FeP_x/NPSC	1.57	216.9	93	0.87-0.96	[23]
$RuCoO_x$	1.54	160	1100 cycles @ 5 mA cm^{-2}	~0.86	[24]
RuCo/NPC	1.68	79.4	16.67 @ 2 mA cm^{-2}	~0.75	[25]
Re-Ni_3S_2/NG/NF	1.58	99	266	~0.88	[26]
NAC@Co_3O_4/NCNTs/CNF	--	267.6	67	0.8--1.25	[27]
Pd-coated (CoFe/NCNTs)	1.60	261	50	0.69	[28]
CoP/Co_3O_4-fC-pPVP	1.58	154	727 @ 5 mA cm^{-2}	~0.75	[29]
CoFeN-NCNTs//CCM	1.63	145	445	0.76	[30]
B-$CoSe_2$@CoNi LDH HNA	1.58	181.5	70 @ 1 mA cm^{-2}	~0.8	[31]
NiCu-MoS_2	1.62	283	133	0.71-0.74	[32]

4. Reference

[1] Jian, J.; Yuan, L.; Qi, H.; Sun, X. J.; Zhang, L.; Li, H.; Yuan, H. M.; Feng, S. H. *ACS Appl. Mater. Inter.* **2018**, 10, 40568.

[2] Jian, J.; H. M. Yuan and et al. *J. Mater. Chem. A* **2021**, 9, 7586-7593.

[3] Kresse, G.; Furthmüller, J. *Comput. Mater. Sci.* **1996**, 6, 15-50.

[4] Kresse, G.; Furthmüller, J. *Phys. Rev. B* **1996**, 54, 11169-11186.

[5] Perdew, J. P.; Burke, K.; Ernzerhof, M. *Phys. Rev. Lett.* **1996**, 77, 3865-3868.

[6] Kresse, G.; Joubert, D. *Phys. Rev. B* **1999**, 59, 1758-1775.

[7] Blöchl, P. E. *Phys. Rev. B* **1994**, 50, 17953−17979.

[8] Monkhorst, H. J.; Pack, J. D. *Phys. Rev. B*, **1976**, 13, 5188-5192.

[9] Hu, X. L.; Pan, F. S.; and et al. *Green Energy Environ.* **2023**, 8, 601-611.

[10] He, B.; Su, Z.; and et al. *CrystEngComm* **2021**, 23, 3861.

[11] Muthurasu, A.; Kim, H. Y.; and et al. *Nano Energy*, **2021**, 106238.

[12] Duan, X. D.; Zheng, H. G.; and et al. *J. Energy. Chem.* **2021**, 56, 290-298.

[13] Liu, Q.; Yang, W. Y. and et al. *Chemical Eng. J.* **2021**, 423, 130313.

[14] Liu, J.; Leung, K. H. and et al. *ACS Appl. Mater. Interfaces* **2022**, 14, 4399-4408.

[15] Liu, N.; Guan, J. Q.; and et al. *Electrochimica Acta* **2021**, 380, 138215.

[16] Wang, S. J.; Hu, Y.; and et al. *Appl. Catal., B* **2021**, 298, 120512.

[17] Wang, A. S.; Wang, W. C.; and et al. *Appl. Catal., B* **2021**, 281, 119514.

[18] Wu, Z. X.; Wang, L.; and et al. *Chinese J. Catal.* **2023**, 46, 36-47.

[19] Zhao, S. L.; Zhu, Z. H.; and et al. *Small* **2023**, 2302414.

[20] Wang, F. L.; Chen, Y. L.; and et al. *J. Power Sources* **2022**, 521, 230925.

[21] Yao, Y.-F.; Xiao, X.-Y.; and et al. *Catal. Sci. Technol.* **2023**, 13, 6321-6330.

[22] Zhang, Y. L.; Guo, S. H.; and et al. *Composites Part B* **2023**, 253, 110575.

[23] Li, P.; Liu, S.; and et al. *Chemical Eng. J.* **2021**, 421, 129704.

[24] Zhou, C. H.; Zhang, R. F.; and et al. *Nano Lett.* **2021**, 21, 9633-9641.

[25] Pei, Y.; Wang, J. C.; and et al. *Chem. Commun.* **2021**, 57, 1498-1501.

[26] Han, X. T.; Li, N. N.; and et al. *Composites Part B* **2022**, 234, 109670.

[27] Yao, X. Y.; Zhang, W. M.; and et al. *Inorg. Chem. Front.* **2022**, 9, 2517-2529.

[28] Manjunatha, R.; Zhang, J. J.; and et al. *Green Energy Environ.* **2022**, 7, 933-947.

[29] Liu, Z.; Xu, W. J.; and et al. *Electrochimica Acta* **2022**, 412, 140134.

[30] Zhou, G. Z.; Wang, L.; and et al. *Adv. Funct. Mater.* **2021**, 2107608.

[31] Song, J. N.; Peng, S. J.; and et al. *Adv. Sci.* **2022**, 2104522.

[32] Kumar, M.; Nagaiah, T. C.; and et al. *J. Mater. Chem. A* **2023**, 11, 18336-18348.